Tubulin tyrosination is a major factor affecting the recruitment of CAP-Gly proteins at microtubule plus ends

Leticia Peris,[1] Manuel Thery,[2] Julien Fauré,[1] Yasmina Saoudi,[1] Laurence Lafanechère,[1] John K. Chilton,[3] Phillip Gordon-Weeks,[3] Niels Galjart,[4] Michel Bornens,[2] Linda Wordeman,[5] Juergen Wehland,[6] Annie Andrieux,[1] and Didier Job[1]

[1]Laboratoire du Cytosquelette, Institut National de la Santé et de la Recherche Médicale U366, Département Réponse et Dynamique Cellulaire, Commisariat à l'Energie Atomique Grenoble, 38054 Grenoble, France
[2]Biologie du Cycle Cellulaire et de la Motilité, UMR144, Centre National de la Recherche Scientifique, Institut Curie, 75248 Paris, Cedex 05, France
[3]Medical Research Council Centre for Developmental Neurobiology, King's College London, London SE1 1UL, England, UK
[4]Department of Cell Biology and Genetics, Erasmus Medical Center, 3000 DR Rotterdam, Netherlands
[5]Department of Physiology and Biophysics, University of Washington, Seattle, WA 98195
[6]Department of Cell Biology, German Research Center for Biotechnology, D-38124 Braunschweig, Germany

Tubulin-tyrosine ligase (TTL), the enzyme that catalyzes the addition of a C-terminal tyrosine residue to α-tubulin in the tubulin tyrosination cycle, is involved in tumor progression and has a vital role in neuronal organization. We show that in mammalian fibroblasts, cytoplasmic linker protein (CLIP) 170 and other microtubule plus-end tracking proteins comprising a cytoskeleton-associated protein glycine-rich (CAP-Gly) microtubule binding domain such as CLIP-115 and p150 Glued, localize to the ends of tyrosinated microtubules but not to the ends of detyrosinated microtubules.

In vitro, the head domains of CLIP-170 and of p150 Glued bind more efficiently to tyrosinated microtubules than to detyrosinated polymers. In TTL-null fibroblasts, tubulin detyrosination and CAP-Gly protein mislocalization correlate with defects in both spindle positioning during mitosis and cell morphology during interphase. These results indicate that tubulin tyrosination regulates microtubule interactions with CAP-Gly microtubule plus-end tracking proteins and provide explanations for the involvement of TTL in tumor progression and in neuronal organization.

Introduction

In most eukaryotic cells, the C terminus of α-tubulin is subject to a cycle of detyrosination–tyrosination, in which the C-terminal tyrosine residue of α-tubulin is sequentially cleaved from the peptide chain by tubulin carboxypeptidase (TCP) and readded to the chain by the tubulin-tyrosine ligase (TTL; Barra et al., 1988). In both animal models and human cancers, TTL is often suppressed during tumor growth, indicating that TTL suppression and resulting tubulin detyrosination represent a strong selective advantage for proliferating transformed cells (Lafanechere et al., 1998; Mialhe et al., 2001). In whole animals, TTL is

essential for neuronal organization: TTL-null mice die within hours after birth because of the disorganization of vital neuronal circuits (Erck et al., 2005). In *Saccharomyces cerevisiae*, where the tyrosination cycle does not occur but where the structure of the α-tubulin C terminus is conserved, removal of the C-terminal aromatic residue of α-tubulin (a phenylalanine in yeast instead of a tyrosine) disables the interaction of microtubule (MT) plus ends with Bik1p, the yeast equivalent of the mammalian MT plus-end tracking protein cytoplasmic linker protein (CLIP) 170 (Badin-Larcon et al., 2004). Consistent with a role of tubulin tyrosination in CLIP-170 localization, CLIP-170 is mislocalized in TTL-null neurons, being absent from the distal part of neurites and from growth cones (Erck et al., 2005).

In this study, we have used TTL-null fibroblasts, in which, in contrast with neurons, individual MTs are distinct, to probe the influence of tubulin tyrosination on the recruitment of CLIP-170 and of other MT plus-end proteins (+TIPs) at MT ends.

Correspondence to Didier Job: didier.job@cea.fr

Abbreviations used in this paper: CAP-Gly, cytoskeleton-associated protein glycine-rich; CLASP, CLIP-associating protein; CLIP, cytoplasmic linker protein; HD, head domain; MCAK, mitotic centromere-associated kinesin; MEF, mouse embryonic fibroblast; MT, microtubule; TTL, tubulin-tyrosine ligase; TCP, tubulin carboxypeptidase; WT, wild type.

The online version of this article contains supplemental material.

We find that tubulin tyrosination is important for proper localization of +TIPs such as CLIP-170, CLIP-115, or p150 Glued, which comprise at least one cytoskeleton-associated protein glycine-rich (CAP-Gly) MT binding motif (Carvalho et al., 2003; Akhmanova and Hoogenraad, 2005), whereas other +TIPs, such as EB1, EB3, CLIP-associating protein (CLASP), or mitotic centromere-associated kinesin (MCAK), interact similarly with tyrosinated or detyrosinated polymers. We provide evidence that TTL suppression and resulting tubulin detyrosination induce abnormalities in spindle positioning and in cell morphology.

Results

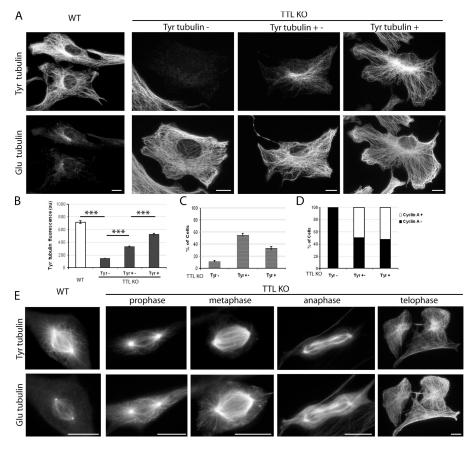### Tubulin tyrosination in wild-type (WT) and TTL-null fibroblasts

TTL-null cells contain massive amounts of detyrosinated (Glu) tubulin but also variable amounts of tyrosinated (Tyr) tubulin originating from tubulin synthesis (Erck et al., 2005). Here, when double stained for Tyr and Glu tubulin, interphasic WT cells displayed extensive tyrosination of cytoplasmic MTs, with only a small subset of Glu MTs (Fig. 1 A), known to correspond to poorly dynamic polymers (Gundersen et al., 1984; Kreis, 1987; Wehland and Weber, 1987). Interphase TTL-null fibroblasts contained extensive arrays of Glu MTs and variable amounts of Tyr tubulin (Fig. 1 A). In four independent experiments, 11–15% of TTL-null fibroblasts displayed only background signal when stained with Tyr tubulin antibody

(Fig. 1, A–C, Tyr−), 50–60% of the cells showed partial staining of the MT network (Fig. 1, A–C, Tyr+−), and 30–40% of the cells showed distinct staining of the whole MT network (Fig. 1, A–C, Tyr+). All Tyr− cells were also negative for the G2/S marker cyclin A, indicating that all were G1 cells (Fig. 1 D). When MT stability was probed using cell exposure to nocodazole (unpublished data), the bulk of cytoplasmic MTs in all WT or TTL-null cells were nocodazole sensitive, indicating that in interphase TTL-null cells, MT detyrosination was not due to increased MT stability.

In WT mitotic cells, Tyr tubulin antibody stained both the central region of the spindle and the cell periphery, which contains a free tubulin pool and astral MTs. The Glu tubulin signal was low, with a distinct staining of centrioles (Fig. 1 E). In TTL-null mitotic cells, the Tyr tubulin signal was evident in prophase and remained strong through the whole mitotic process (Fig. 1 E). In metaphase or anaphase cells, spindle MTs were stained with both Tyr and Glu tubulin antibody. Interestingly, in all metaphase cells examined, Tyr tubulin staining was apparently enriched in the core region of the spindle, with no detectable signal at the periphery of the cell, where Glu tubulin staining yielded both a diffuse signal corresponding to the soluble tubulin pool and a distinct staining of astral MTs.

Collectively, these results indicate that tubulin detyrosination is maximal in interphase TTL-null fibroblasts, where G1 cells can lack detectable Tyr tubulin. Tyr tubulin is present in G2/S and throughout mitosis. Additionally, in metaphase TTL-null cells, Tyr tubulin seems to be preferentially recruited to core

Figure 1. **Tubulin tyrosination in WT or TTL-null fibroblasts.** (A) Double immunostaining of Tyr and Glu tubulin in WT or TTL-null (TTL KO) interphase fibroblasts. MT network of WT fibroblasts was mainly composed of Tyr tubulin. TTL-null fibroblasts contained extensive arrays of Glu MTs and variable amounts of Tyr tubulin. Some cells (Tyr−) showed only background signal. Other cells showed distinct but incomplete staining of the MT network (Tyr+−). Finally, a proportion of the cells (Tyr+) showed staining of most of the MT network. (B) Fluorescence intensity of Tyr tubulin signal (arbitrary units) in WT (n = 90), TTL-null Tyr− (n = 90), TTL-null Tyr+− (n = 32), and TTL-null Tyr+ fibroblasts (n = 58). Fluorescence intensity was <200 au in Tyr− cells and >400 au in Tyr+ cells. (C) Proportions of Tyr−, Tyr+−, and Tyr+ cells in a TTL-null population (n = 308). Error bars indicate SEM. (D) Proportion of cyclin A+ cells (S/G2 cells) in Tyr−, Tyr+−, or Tyr+ interphase TTL-null fibroblasts (n = 125). Note that all the Tyr− cells were also cyclin A−. (E) Double immunostaining of Tyr and Glu tubulin in WT and TTL-null mitotic fibroblasts. Note that in metaphase TTL-null mitotic fibroblasts, Tyr tubulin is only detectable in central spindle MTs, whereas astral MTs and the soluble tubulin pool are composed of Glu tubulin. More than 50 mitotic cells were examined in each genotype. Bars, 10 μm.

spindle MTs, which include the slowly treadmilling kinetochore-to-pole fibers (Mitchison, 1989), whereas the soluble tubulin pool and the dynamic astral MTs are essentially composed of Glu tubulin.

CLIP-170 localization in WT and TTL-null fibroblasts

Previous evidence has suggested that CLIP-170 association with growing MT plus ends is inhibited by tubulin detyrosination, whereas EB1 localization is unaffected (Badin-Larcon et al., 2004; Erck et al., 2005). To assess CLIP-170 localization as a function of tubulin tyrosination, WT or TTL-null cells were triple labeled with EB1 antibody, CLIP-170 antibody, and Tyr tubulin antibody (Fig. 2, A and B). In WT cells, CLIP-170 co-localized with EB1 in comet-like structures at MT ends. Similar colocalization was observed in Tyr+ TTL-null cells. In contrast, Tyr− TTL-null cells were essentially devoid of CLIP-170 comets. For quantitative analysis of CLIP-170 localization on growing MT plus ends, 30 EB1-labeled MT ends were selected in each individual cell and examined for CLIP-170 labeling, and the percentage of CLIP-170–positive MT ends (CLIP-170+) was determined. All measurements were performed blind to genotype. In interphase WT cells, >87% of the EB1+ MT ends were also positive for CLIP-170 (Fig. 2 C). In TTL-null cells,
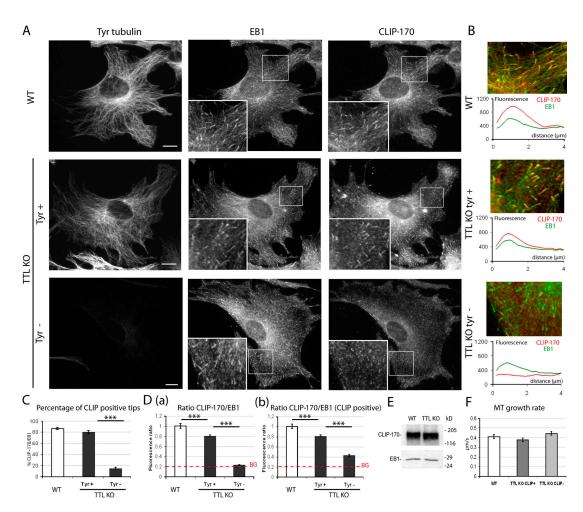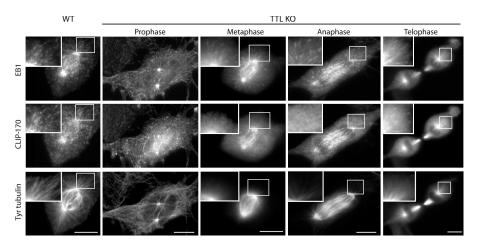

Figure 2. **CLIP-170 localization in WT or TTL-null fibroblasts.** (A) Triple staining of Tyr tubulin, EB1, and CLIP-170 in WT or TTL-null (TTL KO) fibroblasts. MT ends were identified by EB1 labeling. In WT cells, CLIP-170 and EB1 colocalized at MT ends. TTL-null fibroblasts showed several patterns of CLIP-170 distribution depending on Tyr tubulin levels: Tyr+ cells showed CLIP-170 comets at most MT ends, whereas Tyr− cells lacked detectable CLIP-170 comets. Bars, 10 μm. (B, top) High magnification of a region of interest from WT or TTL-null fibroblasts. Merged images show CLIP-170 in red and EB1 in green. Colocalization is shown in yellow. (bottom) Graph of the line scan of fluorescence intensity (arbitrary units) of CLIP-170 (red) and EB1 (green), starting at the end of the MT (distance 0) to 4 μm inwards. (C) Quantitative analysis of CLIP-170 localization in WT or TTL-null fibroblasts. Mean values ± SEM of the percentage of CLIP-170+ ends among EB1 MT ends (% CLIP-170/EB1) in WT ($n = 37$), TTL-null Tyr+ ($n = 30$), and TTL-null Tyr− cells ($n = 41$), respectively. ***, $P < 0.001$ (t test). Less than 15% of MT ends were detectably labeled with CLIP-170 antibody in Tyr− cells, whereas the proportion of CLIP+ ends was never <80% in WT or in TTL-null Tyr+ cells. (D) Fluorescence ratios of CLIP-170 and EB1 in WT or TTL-null fibroblasts. (a) For each cell type, 90 EB1+ comets were chosen, and mean fluorescence intensities were measured for EB1 and CLIP-170. Background signal (BG) corresponded to the mean fluorescence intensity of a straight line drawn across a Tyr− cell. (b) Same as panel a, restricting the analysis to MT ends scored as CLIP+ in WT ($n = 90$), TTL-null Tyr+ ($n = 90$), and TTL-null Tyr− ($n = 56$) cells. Even when CLIP-170 comets were visible, CLIP-170 signal was markedly diminished in TTL-null cells compared with WT cells. (E) Western blot analysis of CLIP-170 and of EB1 content in WT or TTL-null fibroblast extracts. Equal amounts of proteins were loaded in each line. (F) MT growth rate measurement in WT or TTL-null cells (mean ± SEM). Cells were double transfected with GFP–CLIP-170 and EB3-RFP cDNAs. In all cells, MT ends were decorated with EB3-RFP, and the velocity of MT growth was measured using video microscopy. TTL-null cells were classified as CLIP+ when the percentage of CLIP-170/EB3 was ≥40% or as CLIP− when the percentage of CLIP-170/EB3 was ≤15%. WT ends, $n = 70$; TTL-null CLIP+ ends, $n = 70$; TTL-null CLIP− ends, $n = 84$. See Videos 1–3, available at http://www.jcb.org/cgi/content/full/jcb.200512058/DC1.
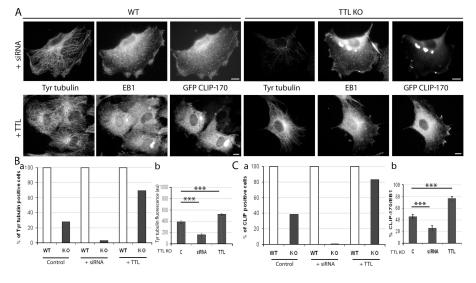
Figure 3. CLIP-170, EB1, and Tyr tubulin distribution in mitotic cells. WT or TTL-null (TTL KO) fibroblasts were triple labeled with EB1, CLIP-170, and Tyr tubulin antibodies. At least 30 mitotic cells were examined in each genotype. In WT mitotic cells, numerous CLIP-170 and EB1 comets were evident. CLIP-170 and EB1 comets were also conspicuous in prophase and telophase TTL-null cells with extensive arrays of Tyr MTs. In metaphase and anaphase TTL-null cells, CLIP-170 labeled the core spindle region as in WT cells, although no distinct CLIP-170 comets were observed at the cell periphery, where MTs lacked Tyr tubulin. Bars, 10 μm.

a strong relationship between tubulin tyrosination and CLIP-170 localization was evident, with only 14% of the EB1-labeled MT ends being also positive for CLIP-170 in cells classified as Tyr−, compared with 80% of positive ends in cells classified as Tyr+ (Fig. 2 C). CLIP-170/EB1 fluorescence ratios were higher in WT cells than in Tyr+ TTL-null cells and close to background levels in Tyr− TTL-null cells (Fig. 2 D a). The few CLIP-170 comets visible in Tyr− cells had low CLIP-170 signal compared with CLIP-170+ comets in Tyr+ or WT cells (Fig. 2 D b). In a series of control experiments, we checked that CLIP-170 expression levels were not different in WT cells compared with TTL-null cells (Fig. 2 E). We also checked by cyclin A staining that a similar proportion of G1 (75%) and G2/S cells were present in WT or TTL-null cell populations and that in WT cells, CLIP-170 localization was not detectably different in cyclin A− cells compared with cyclin A+ cells (unpublished data). CLIP-170 localization at growing MT plus ends could be influ-

enced by MT growth rates. We used video microscopy and fluorescent protein constructs to test whether MT growth rates differed as a function of the tubulin tyrosination status. In cells double transfected with GFP–CLIP-170 and EB3-RFP, GFP–CLIP-170 behaved as endogenous CLIP-170, associating with MT ends in WT cells and in Tyr+ TTL-null cells but not in Tyr− TTL-null cells, indicating that tyrosination affects CLIP-170 localization within a large range of protein expression levels (Fig. S1, available at http://www.jcb.org/cgi/content/full/jcb.200512058/DC1). We measured MT growth rates in double-transfected cells by video microscopy tracking of EB3-RFP–labeled MT ends. Interestingly, we observed similar MT growth rates in WT cells compared with TTL-null cells, whether or not CLIP-170 was correctly localized (Fig. 2 F and Videos 1–3), indicating that CLIP-170 mislocalization is not due to impaired MT growth in TTL-null cells but likely reflects an influence of tubulin detyrosination by itself.

Figure 4. Inhibition or rescue of tubulin tyrosination in TTL-null fibroblasts. (A) WT or TTL-null (TTL KO) fibroblasts were transfected with GFP–CLIP-170 cDNA and either treated with siRNA against α-tubulin (+siRNA) or cotransfected with TTL cDNA (+TTL). In control experiments, cell transfection with scramble siRNA or TTL vector alone gave similar results, shown as control. Cells were triple stained with Tyr tubulin, EB1, and GFP antibodies. Bars, 10 μm. (B, a) Percentage of Tyr+ cells (mean fluorescence intensity > 400; Fig. 1) in a WT or TTL-null population nontreated (control WT, n = 52; control TTL-null, n = 98), treated with siRNA against Tyr tubulin (+siRNA WT, n = 50; +siRNA TTL-null, n = 82), or transfected with TTL cDNA (+TTL WT, n = 50; +TTL TTL-null, n = 96). In WT cells, treatments had no effect on tubulin tyrosination. In TTL-null cells, siRNA treatment drastically suppressed the percentage of Tyr+ cells as compared with control conditions, whereas the percentage of Tyr+ cells increased to 70% in double GFP–CLIP-170/TTL cDNA transfection. (b) Comparison of Tyr tubulin fluorescence (arbitrary units; mean ± SEM) in TTL-null fibroblasts, in nontreated cells, in cells treated with siRNA against α-tubulin, and in cells cotransfected with TTL cDNA. ***, P < 0.001 (t test). (C, a) Percentage of CLIP+ cells (>75% of CLIP+ ends) in a WT or TTL-null population nontreated (control WT, n = 52; control TTL-null, n = 98), treated with α-tubulin siRNA (+siRNA WT, n = 50; +siRNA TTL-null, n = 82), or transfected with TTL cDNA (+TTL WT, n = 50; +TTL TTL-null, n = 96). CLIP+ cells were defined as cells showing >75% of CLIP+ ends. In TTL-null cells, no CLIP+ cell was observed after exposure to siRNA. In contrast, >80% of TTL-null cells were CLIP+ after TTL cDNA transfection. (b) Mean values ± SEM of the percentage of CLIP-170/EB1 in TTL-null fibroblasts in nontreated cells, in cells treated with siRNA against α-tubulin, and in cells cotransfected with TTL cDNA. ***, P < 0.001 (t test).

In WT mitotic cells, many CLIP-170 and EB1 comets were visible (Fig. 3). In TTL-null mitotic cells, which contain abundant Tyr tubulin, CLIP-170 comets were also conspicuous (Fig. 3). However, interestingly, in TTL-null metaphase cells, whereas CLIP-170 staining of the core spindle was similar to that observed in WT cells (and as found in previous work [Tanenbaum et al., 2006]), CLIP-170 comets were undetectable at the cell periphery, compatible with a lack of CLIP-170 interaction with the detyrosinated astral MTs (see Figs. 2 and 3). Comets reappeared at the cell periphery in telophase, presumably when Tyr tubulin from the disassembling core spindle MTs redistributed among astral MTs. Collectively, our results indicate that in TTL-null cells, MT tyrosination is critical for CLIP-170 association with MT ends.

Effect of the inhibition or rescue of tubulin tyrosination on CLIP-170 localization in TTL-null fibroblasts

The evidence we have shown indicates a strong correlation between MT tyrosination and CLIP-170 localization. We used experimental manipulation of the tubulin tyrosination level in TTL-null cells to test the causal nature of this relationship. For Tyr tubulin depletion, we made use of previously described α-tubulin siRNAs, which suppress α-tubulin synthesis and thereby the Tyr tubulin pool in TTL-null cells (Erck et al., 2005). WT controls or TTL-null fibroblasts were transfected with GFP–CLIP-170 and exposed to α-tubulin siRNA. These siRNAs have no effect on tubulin tyrosination in WT cells, where tubulin is tyrosinated by TTL. In these cells, the MT network was somewhat disorganized (Erck et al., 2005; Fig. 4 A), but MT ends remained uniformly positive for GFP–CLIP-170. In contrast, α-tubulin siRNAs induced extensive suppression of Tyr tubulin in TTL-null cells (Fig. 4, A and B). Accordingly, we did not observe CLIP-positive cells among siRNA-treated TTL-null fibroblasts (Fig. 4, A and C). Conversely, cotransfection of TTL-null cells with TTL cDNA together with GFP–CLIP-170 dramatically increased both the level of MT tyrosination and the proportion of cells with CLIP-170 at MT ends (Fig. 4). We observed similar results with endogenous protein as with transfected GFP–CLIP-170 (unpublished data). In control experiments, no change in the proportion of G1 versus G2/S cells was detectable after the various cell treatments. These results strongly indicate that CLIP-170 mislocalization is causally related to tubulin detyrosination in TTL-null cells.

Differential binding of CLIP-170 head domain (HD) to tyrosinated and detyrosinated MTs

Is the influence of tubulin tyrosination on CLIP-170 interaction with MTs direct or indirect? To approach this question, we examined the interaction of the CLIP-170 HD, which contains the
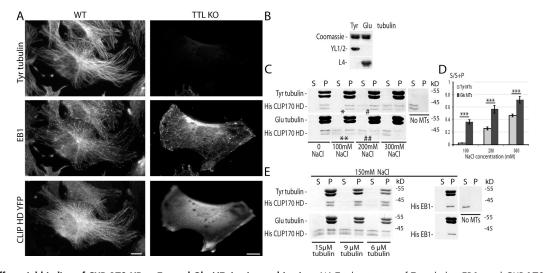

Figure 5. **Differential binding of CLIP-170 HD to Tyr and Glu MTs in vivo and in vitro.** (A) Triple staining of Tyr tubulin, EB1, and CLIP-170 HD in WT or TTL-null (TTL KO) fibroblasts transfected with CLIP-170–HD–YFP cDNA. In WT cells, overexpressed CLIP-170–HD–YFP decorated the whole MT network and accumulated at MT ends. In Tyr− TTL-null cells, CLIP-170-HD-YFP remained soluble in the cytoplasm. Bar, 10 μm. (B) Tyr and Glu tubulin levels in the immuno-affinity-isolated tubulin. Equal amounts of affinity-purified Tyr or Glu tubulin were loaded onto an SDS-PAGE gel and stained with Coomassie blue or immunoblotted with anti–Tyr tubulin (YL1/2 antibody) or anti–Glu tubulin (L4 antibody). (C) MT binding assay. CLIP-170 HD (His–CLIP-170 HD) was incubated alone (no MTs) or copolymerized with Tyr or Glu tubulin. Tyr and Glu MTs were stabilized with taxol and incubated with increasing concentrations of NaCl, as indicated. After centrifugation, equal amounts of supernatants (S) and pellets (P) were loaded onto an SDS-PAGE gel and stained with Coomassie blue. His–CLIP-170 HD is visible as a protein doublet with a molecular mass of ~40 kD as previously observed in Scheel et al. (1999). In the presence of 100 mM NaCl, the bulk of His–CLIP-170 HD remained bound to Tyr MTs (*), whereas it began to be eluted from Glu MTs (**). In the presence of 200 mM NaCl, only a small proportion of His–CLIP-170 HD was eluted from Tyr MTs (#), whereas more than the half of His–CLIP-170 HD was eluted from Glu MTs (##). Tyr and Glu MT final concentration was 12 μM, and His–CLIP-170 HD final concentration was 5 μM. (D) Quantitative analysis of His–CLIP-170 HD elution from Tyr or Glu MTs at different NaCl concentrations. Mean value ± SEM of His–CLIP-170 HD present in the supernatant fraction (S/S+P) of Tyr or Glu MTs (n = 12). ***, P < 0.001 (t test). (E) Analysis of MT binding in function of tubulin concentration at 150 mM NaCl. His–CLIP-170 HD (final concentration of 5 μM) was copolymerized with decreasing concentrations of Tyr or Glu tubulin as indicated. Taxol MTs were incubated with 150 mM NaCl and centrifugated. Supernatants and pellets were loaded onto an SDS-PAGE gel and stained with Coomassie blue. The bulk of His–CLIP-170 HD remained bound to Tyr MTs, whereas it was partially eluted from Glu MTs at each tubulin concentration in the presence of 150 mM NaCl. At the same NaCl concentration, His-EB1 (final concentration of 5 μM) remained associated to both Tyr and Glu MTs.

MT binding domain CAP-Gly (Perez et al., 1999; Scheel et al., 1999), with Tyr or Glu MTs, both in vivo and in vitro. When WT fibroblasts were transfected with CLIP-170 HD fused with YFP (CLIP-170–HD–YFP), CLIP-170–HD–YFP formed comets at MT ends and decorated MTs lengthwise (Fig. 5 A). Interestingly, the comets and the lengthwise MT signal were both lacking in TTL-null Tyr− cells (Fig. 5 A). We then tested whether a differential binding of CLIP-170 HD to Tyr or Glu MTs could be reconstituted in purified systems in vitro. CLIP-170 HD (His–CLIP-170 H1; Scheel et al., 1999) was added in substoechiometric amounts to solutions of affinity-purified Tyr or Glu tubulin (Paturle et al., 1989). Subsequently, tubulin poly-

merization was initiated and taxol was added to stabilize MTs. At low ionic strength, CLIP-170 HD was quantitatively absorbed on both Tyr and Glu MTs. We then tested the effect of increasing NaCl concentrations. Taxol-stabilized MTs were then exposed to increasing NaCl concentrations before the cosedimentation assay of CLIP-170 with MTs (Bulinski et al., 1999). His–CLIP-170 HD showed a double band with a molecular mass of 40 kD as observed in Scheel et al. (1999). Interestingly, CLIP-170 HD began to be eluted from Glu MTs at 100 mM NaCl (Fig. 5, C [**] and D) and was further dissociated from Glu MTs at 200 mM NaCl (Fig. 5, C [##] and D), whereas at similar NaCl concentrations, the bulk of CLIP-170 HD
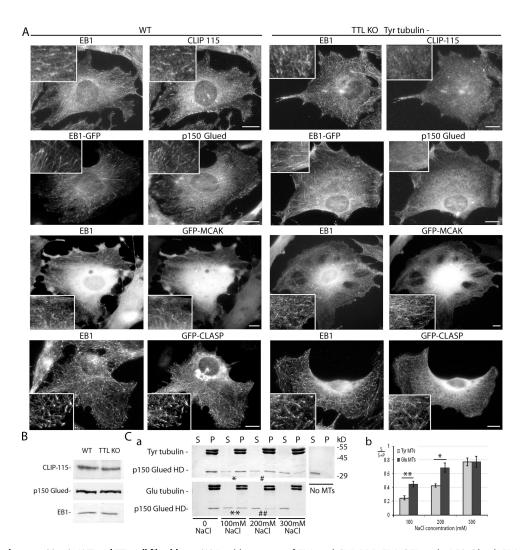

Figure 6. **MT end composition in WT and TTL-null fibroblasts.** (A) Double staining of EB1 and CLIP-115, EB1-GFP and p150 Glued, EB1 and GFP-MCAK, or EB1 and GFP-CLASP in WT or TTL-null (TTL KO) cells. In WT fibroblasts, endogenous CLIP-115 and p150 Glued showed a comet-like distribution at MT ends. In TTL-null fibroblasts, Tyr−, CLIP-115, and p150 Glued did not decorate MT ends and showed a diffuse distribution in the cytoplasm. GFP-MCAK and -CLASP equally decorated MT ends in WT or TTL-null Tyr− cells. More than 50 cells were examined in each genotype for each condition. Bars, 10 μm. (B) Western blot analysis of CLIP-115, p150 Glued, and EB1 content in a WT or TTL-null fibroblast extract. Equal amounts of proteins were loaded in each line. (C, a) MT binding assay of p150 Glued HD. p150 Glued HD was copolymerized with Tyr or Glu tubulin. Tyr and Glu MTs were stabilized with taxol and incubated with increasing concentrations of NaCl, as indicated. Equal amount of supernatants (S) and pellets (P) were loaded onto an SDS-PAGE gel and stained with Coomassie blue. p150 Glued HD showed a band with a molecular mass close to 30 kD. In the presence of 100 mM NaCl, a small proportion of p150 Glued HD eluted from Tyr MTs (*), whereas about half of the p150 Glued HD eluted from Glu-MTs (**). In the presence of 200 mM NaCl, less than a half of p150 Glued HD eluted from Tyr MTs (#), whereas the main proportion of p150 Glued HD eluted from Glu MTs (##). Tyr and Glu MT final concentration was 12 μM, and p150 Glued HD final concentration was 5 μM. (b) Quantitative analysis of p150 Glued HD elution from Tyr or Glu MTs at different NaCl concentrations. Mean value ± SEM of p150 Glued HD present in the supernatant fraction (S/S+P) of Tyr or Glu MTs ($n = 7$). **, $P < 0.01$; *, $P < 0.05$ (t test).
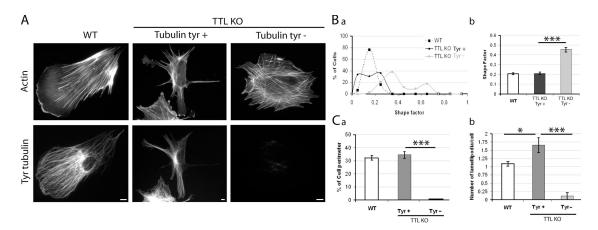
was still associated with Tyr MTs (Fig. 5, C [* and #] and D). Interestingly, the differential binding of CLIP-170 HD to Glu or Tyr MTs occurred at NaCl corresponding to the intracellular NaCl concentration (150 mM). CLIP-170 HD binding to Tyr and Glu MTs was then tested at different tubulin concentrations at 150 mM NaCl. CLIP-170 HD was present in supernatants at all concentrations with Glu MTs, whereas it only appears in supernatants at close to saturating concentrations (5 μM CLIP-170 HD for 6 μM tubulin) with Tyr MTs (Fig. 5 E). At the same NaCl concentration, a His-EB1 construct was still quantitatively absorbed on both Tyr and Glu MTs (Fig. 5 E) and began to be eluted only at 500 mM NaCl, similarly from Tyr or Glu MTs (not depicted). Collectively, these results indicate that tubulin tyrosination interferes directly with CLIP-170 interaction with MTs but does not affect other +TIPs with different MT binding domain, such as EB1.

Tubulin tyrosination affects MT interaction with CAP-Gly end-tracking proteins

The CAP-Gly MT binding domain of CLIP-170 is also present in the MT end-tracking proteins CLIP-115 and p150 Glued. The HDs of CLIP-115 and -170 are homologous, and in this study, in all qualitative and quantitative cellular assays, endogenous CLIP-115 or the GFP–CLIP-115 construct behaved like CLIP-170, binding to Tyr but not to Glu MTs (Fig. 6 A and not depicted). Interestingly, endogenous p150 Glued or the EGFP–p150 Glued construct also behaved like CLIP-170 in similar assays (Fig. 6 A and not depicted). In in vitro MT binding assays, a differential binding of p150 Glued to Tyr or Glu MTs was always detectable, although less evident than in the case of CLIP-170 (Fig. 6, A and C). We have shown that, in contrast, EB1 and EB3, two highly related proteins whose MT binding domain does not comprise a CAP-Gly motif, are unaffected by MT tyrosination in vivo (Figs. 2–6 and Videos 1–3) and in vitro

(Fig. 5 E). MCAK, which has recently been shown to end track MTs (Moore et al., 2005), and CLASPs, a previously identified +TIP (Akhmanova et al., 2001), also decorated MT plus ends in Tyr− TTL-null cells (Fig. 6 A). We conclude that tubulin tyrosination affects MT interactions with CAP-Gly +TIPs in the absence of obvious effects on the behavior of other +TIPs. TTL-null cells then offered an original system in which a single amino acid deletion in α-tubulin, not affecting protein folding, specifically disrupted the interaction of MTs with CAP-Gly +TIPs. The most obvious cellular consequences of such a disruption are shown in the next sections.

Cell morphology and polarization in TTL-null fibroblasts

CAP-Gly +TIPs are involved in MT interactions with the cell membrane (Brunner and Nurse, 2000; Akhmanova et al., 2001; Komarova et al., 2002; Carvalho et al., 2003; Busch and Brunner, 2004; Lansbergen et al., 2004; Akhmanova and Hoogenraad, 2005; Mimori-Kiyosue et al., 2005), and there is evidence that tubulin detyrosination affects cell morphogenesis in neurons (Erck et al., 2005). In nonneuronal cells, it has been suggested that the presence of CLIP-170 at MT ends is important for MT-dependent regulations of actin assemblies, such as lamellipodia (Fukata et al., 2002; Gundersen, 2002). Upon examination, WT fibroblasts often displayed a distinct polarity by extending a single lamellipodium (Fig. 7 A), as expected from the behavior of a normal fibroblast, which extend a lamellipodium in the direction of cell migration (Pollard and Borisy, 2003). Similar polarized lamellipodium extension was never observed in Tyr− TTL-null cells, which showed a more or less regular round shape (Fig. 7 A), whereas Tyr+ TTL-null fibroblasts often displayed numerous extensions with several large lamellipodia, resulting in a conspicuously irregular cell shape (Fig. 7 A). We used a standard shape factor (defined by $4\pi A/P^2$,
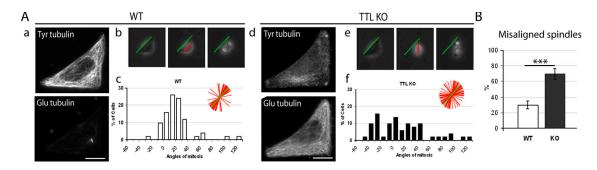

Figure 7. **Morphological analysis of WT or TTL-null fibroblasts.** (A) Double staining of actin and Tyr tubulin in WT or TTL-null (TTL KO) fibroblasts. WT cells often showed a polarized morphology with a large lamellipodium. Tyr+ TTL-null fibroblasts often displayed two or more lamellipodia. In contrast, Tyr− TTL-null fibroblasts lacked distinct polarization. Bars, 10 μm. (B) The graph depicts morphology. A shape factor (4π area/perimeter^2) was determined in WT or TTL-null fibroblasts. (a) Shape factor distribution in WT ($n = 43$), TTL-null Tyr+ ($n = 36$), or TTL-null Tyr− fibroblasts ($n = 34$). (b) Shape factor mean values ± SEM. Compared with WT or Tyr+ TTL-null fibroblasts, Tyr− TTL-null cells exhibited a significant increase in the shape factor. ***, $P < 0.001$ (t test). (C, a) Quantitative analysis of the percentage of cell perimeter occupied by lamellipodia in WT, Tyr−, or Tyr+ TTL-null cells. (b) Number of lamellipodia per cell in WT, Tyr−, or Tyr+ TTL-null cells. Tyr− TTL-null cells often displayed no lamellipodia extensions. In contrast, Tyr+ TTL-null cells exhibited an increased number of large lamellipodia extensions compared with WT fibroblasts (WT, $n = 68$; Tyr−, $n = 20$; Tyr+, $n = 38$). ***, $P < 0.001$; *, $P < 0.05$ (t test).

Figure 8. **Mitotic spindle orientation in WT or TTL-null fibroblasts.** (A) Double immunostaining of Tyr and Glu tubulin in a WT (a–c) or TTL-null (TTL KO; d–f) interphase fibroblasts grown on an L-shaped fibronectin micropattern. (b and e) Example of time-lapse acquisition of a WT (b) or a TTL-null (e) cells during mitosis. Time-lapse pictures were used to measure the mitotic angle (red line) in function of the hypotenuse angle of the pattern (green line). (c and f) The distribution of mitotic angles in WT (c; n = 50) and TTL-null (f; n = 51) populations is shown. TTL-null cells showed a disperse spindle orientation compared with WT cells. (B) Percentages of misaligned spindles (spindle angle deviating by >15° from the median value in WT (n = 50) or TTL-null populations (n = 51). TTL-null fibroblasts exhibited a large increase in misaligned spindles compared with WT cells. ***, P < 0.001 (t test). Bars, 10 μm.

where A is the area and P the perimeter) for quantitative analysis of cell shape. This shape factor varies from 0 to 1, for elongated or circular shapes, respectively. Compared with WT cells, Tyr− TTL-null cells had an increased shape factor, indicative of a more regular, round shape (Fig. 7 B). Among WT cells, shape factors were similar between G1 in G2/S cells (unpublished data). Tyr+ TTL-null cells had a mean shape factor comparable to that of WT cells, although there was an excess population of cells with a low shape factor (Fig. 7 B), indicative of irregular and elongated cell shape.

In a further quantitative analysis, the ratio of the perimeter of large lamellipodia extensions to the total cell perimeter was dramatically diminished in Tyr− TTL-null cells compared with other cells (Fig. 7 C a), and the number of large lamellipodia extensions per cell was increased in Tyr+ TTL-null cells, compared with WT cells (Fig. 7 C b). We conclude that cell morphology is perturbed in TTL-null cells, apparently because of abnormalities in cell polarization, which seems inhibited in Tyr− cells and disorganized in Tyr+ cells.

Defects in spindle positioning in mitotic TTL-null fibroblasts

Spindle positioning is dependent on +TIP-mediated interactions of astral MTs with the cell cortex (Busson et al., 1998; Carvalho et al., 2003; Akhmanova and Hoogenraad, 2005; Huisman and Segal, 2005). We used printed micropatterns of fibronectin to study spindle positioning in WT or TTL-null fibroblasts. Micropatterns constrain extracellular matrix organization and thereby organization of both actin assemblies and cell adhesions, which are important for spindle positioning (Thery et al., 2005). We observed similar organization of actin assemblies or of cell adhesions in TTL-null cells and WT cells placed on micropatterns (unpublished data). Spindle positioning then depends crucially on astral MT interactions with the metaphase cell cortex (Thery et al., 2005). These interactions involve CAP-Gly +TIPs (Busson et al., 1998), which fail to associate with astral MT ends in TTL-null cells.

The majority of mitotic spindles of WT cells grown on L-shaped patterns were oriented along the hypotenuse (Fig. 8 A, a–c). In contrast, there was a wide dispersion of spindle orientations in TTL-null cells (Fig. 8 A, d–f), with ∼70% of spindles deviating by >15° from the median angle compared with only 30% in WT cells (Fig. 8 B), indicating an impaired control of spindle positioning in TTL-null cells.

Discussion

In this study, we show that tubulin tyrosination is central for MT interaction with CAP-Gly +TIPs and that in cells, TTL suppression and resulting tubulin detyrosination affect spindle positioning and cell morphology. Tyr tubulin is not fully suppressed in TTL-null cells (Erck et al., 2005), where Tyr tubulin arises from synthesis of new tubulin molecules. Tyr tubulin levels vary in interphase cells that can exhibit complete detyrosination. In contrast, mitotic cells always contain Tyr tubulin. The constant presence of Tyr tubulin in mitotic TTL-null cells compared with interphase TTL-null cells is intriguing. We do not know whether this uniform presence of Tyr tubulin reflects an increased tubulin synthesis when cells enter mitosis, an inhibition of TCP, or both.

Based on Tyr and Glu tubulin distributions in metaphase TTL-null cells, our data raise the possibility of a preferential recruitment of Tyr tubulin compared with Glu tubulin in kinetochore-to-pole MTs, with a corresponding enrichment of Glu tubulin in astral MTs and in the soluble tubulin pool. Such a preferential recruitment cannot be explained by a difference in Tyr or Glu MT polymerization properties (Paturle et al., 1989). However, recent work in *Drosophila melanogaster* indicates that tubulin incorporation in the treadmilling kinetochore-to-pole MTs during metaphase does not depend only on the intrinsic polymerization properties of tubulin but also on specific regulations that, in *D. melanogaster*, require CLASP (Maiato et al., 2005). Possibly, tubulin incorporation in kinetochore-to-pole fibers also requires CAP-Gly proteins or other unknown proteins whose interaction with MTs depends on tubulin tyrosination. We do not know whether mitotic cells could tolerate the complete suppression of Tyr tubulin. We have observed extensively detyrosinated mitotic cells in siRNA experiments (unpublished data). In these cells, the spindle was conspicuously disorganized, but we found it hard to know whether spindle anomalies were due to tubulin

detyrosination by itself or to other dysfunctions related to the inhibition of α-tubulin synthesis.

In TTL-null cells, tubulin detyrosination affects the recruitment of CAP-Gly proteins at MT ends, whereas EB1 localization is unaffected. Additionally, we observe that tubulin tyrosination affects the interaction of MTs with CAP- Gly+TIPs in purified systems in vitro. Clearly, as suggested by previous studies (Perez et al., 1999; Galjart and Perez, 2003; Badin-Larcon et al., 2004), CLIP-170 and p150 Glued localization at MT ends depends crucially on direct interactions between these +TIPs and MTs, even if interactions between both proteins and their interaction with EB1 are also involved (Vaughan et al., 1999; Lansbergen et al., 2004; Akhmanova and Hoogenraad, 2005; Hayashi et al., 2005). The remarkable influence of the C-terminal tyrosine of tubulin on tubulin interaction with CAP-Gly +TIPs is reminiscent of a recent structural study of the interaction of EB1, which has the same C terminus as α-tubulin, with p150 Glued (Hayashi et al., 2005). In this study, the terminal tyrosine of the EB1 C terminus had a crucial contribution in EB1 interaction with the CAP-Gly domain of p150 Glued (Hayashi et al., 2005). Very recently, a similar role of the C-terminal tyrosine of EB1 has been reported in the case of EB1 interaction with CLIP-170 (Komarova et al., 2005). Such a conservation of the C-terminal tyrosine function is remarkable because the interaction of p150 Glued with tubulin involves several domains (Culver-Hanlon et al., 2006) and the interaction of EB1 with CLIP-170 also involves protein domains other than the EB1 C terminus (Busch and Brunner, 2004).

It is also remarkable that the role of the C-terminal aromatic residue of EB1 and of α-tubulin in regulating interactions with CAP-Gly +TIPs is conserved among organisms, from yeast to mammals, and may concern additional CAP-Gly proteins (Carvalho et al., 2003; Akhmanova and Hoogenraad, 2005). This may explain the conservation of the α-tubulin extreme C-terminal sequence, which has been intriguing, given that this tubulin sequence is not important for the 3D structure of the protein.

TTL-null cells offer a new and attractive system to evaluate the function of +TIPs' interaction with MT. Within the framework of this study, we have restricted our analysis to the most obvious cellular phenotypes. We find that TTL suppression in fibroblasts compromises spindle positioning in cells placed on a micropatterned matrix. A recent study has shown that metaphase spindle positioning in cells grown on micropatterns depends both on the organization of the extracellular matrix, which is controlled by the micropattern, and on astral MT interactions with cues on the cell cortex (Thery et al., 2005). Such interactions are mediated by molecular complexes involving CLIP-170 (or CLIP-115) and p150 Glued (Busson et al., 1998; Coquelle et al., 2002). It is likely that the inhibition of CAP-Gly +TIPs' interaction with detyrosinated astral MTs in TTL-null cells accounts for the impaired control of spindle positioning.

TTL suppression also affects the control of cell shape and of cellular extensions in fibroblasts. In fully detyrosinated cells (Tyr−), where CAP-Gly proteins do not interact with MT ends, cell polarization is diminished, and this agrees with previous work indicating a central role of CLIP-170 in MT-dependent regulations of actin assemblies (Fukata et al., 2002). In TTL-null cells containing enough Tyr tubulin to localize CAP-Gly +TIPs at MT ends, the cell morphology was still perturbed, with multiple cell extensions and an irregular shape. It may be that there are perturbations of CAP-Gly +TIPs' function in cells where MTs are still extensively detyrosinated and where MT ends associate with diminished levels of CLIP-170 or that tubulin detyrosination affects proteins other than +TIPs. These possibilities are under examination in our laboratories.

What is the relationship of the phenotypes observed in TTL-null fibroblasts with the role of TTL in tumor progression and in brain development? Impaired control of spindle positioning has been proposed as one factor favoring tumor invasiveness (Vasiliev et al., 2004). In TTL-null tissues in mice, putative defects in spindle positioning due to tubulin detyrosination are apparently compensated, possibly through the action of geometrical constraints (Yu et al., 2000). The situation may be different in the brain, where TTL-null mice display a variable degree of ventricle enlargement, indicative of cell loss (Erck et al., 2005). Spindle positioning in neuronal progenitors is a complex and highly regulated process crucial for the control of progenitors' proliferation/differentiation in the neuronal epithelium (Faulkner et al., 2000; Haydar et al., 2003). Spindle positioning could be perturbed in TTL-null mice with resulting abnormalities in neuronal differentiation/proliferation equilibrium. With regard to the control of cell morphology, our data are consistent with studies that indicate an important role of CAP-Gly +TIPs for the control of cell shape (Brunner and Nurse, 2000; Fukata et al., 2002; Gundersen, 2002). Such defects in cell shape control are apparently compensated in TTL-null nonneuronal tissues, which are apparently normal, whereas they are probably deleterious in neurons, which exhibit an erratic time course of neurite extensions (Erck et al., 2005). Neuronal cells may be especially sensitive to defects in cell shape controls, given the extreme size and complexity of neurite extensions. Finally, our data suggest that defects in cell shape may be associated with alterations of cell polarity. Such defects may affect cell motility as well as cell–cell or cell–matrix adhesions, which could be involved in the facilitating effect of tubulin detyrosination on tumor growth.

Our data demonstrate that tubulin tyrosination is required for MT interaction with CAP-Gly proteins but do not give definite clues to understand why a great number of eukaryotic cells developed a tyrosination cycle by introducing a detyrosination reaction. The bulk of tubulin is detyrosinated in differentiated cells (Gundersen and Bulinski, 1986), and it may be that tubulin detyrosination is used to disconnect MT–membrane interactions in terminally differentiated cells that do not need to change shape or to divide any longer. The identification of TCP and subsequent TCP suppression will be necessary for a full understanding of the tyrosination cycle. Clearly, though, this cycle is an important aspect of MT physiology, as it is involved in MT functions that are conserved, vital, and important for tumor progression.

Materials and methods

Antibodies
The following primary antibodies were used: Glu tubulin (Paturle-Lafanechere et al., 1994), Tyr tubulin (clone YL1/2; Wehland and Weber, 1987);

EB1 (BD Biosciences), GFP (Invitrogen), cyclin A (clone CY-A1; Sigma-Aldrich), CLIP-115– or CLIP-170–specific antisera (numbers 2238 and 2360, respectively; Hoogenraad et al., 2000; Coquelle et al., 2002), and p150 Glued (clone 1; BD Biosciences).

Cell culture and immunofluorescence microscopy
Mouse embryonic fibroblasts (MEFs) were prepared from embryonic day 13.5 embryos, as previously described (Erck et al., 2005). Cells were maintained at 37°C with 5% CO_2 and 3% O_2. The experiments shown in the present paper were done using pooled fibroblasts from four different embryos, either WT or TTL null.

To visualize plus-end proteins, cultured fibroblasts were washed in warm PBS and fixed first in freshly prepared −20°C methanol/1 mM EGTA, followed by 4% PFA/4.2% sucrose in PBS at room temperature (20 min for each step). To visualize actin, cells were washed in warm PBS and fixed with 4% PFA/4.2% sucrose in PBS at 37°C, followed by cell permeabilization with 0.1% Triton X-100 in PBS. After incubation with primary antibodies, cells were incubated with Cy3, Cy5 (Jackson ImmunoResearch Laboratories), or Alexa 488 (Invitrogen) secondary antibodies. To visualize F-actin, rhodamine-phalloidin (Invitrogen) was included with the secondary antibody. Lamellipodia were identified as cell extensions showing a strong marginal actin signal.

Images were captured with a charge-coupled device camera (CoolSNAP ES; Roper Scientific) in a straight microscope (Axioskop 50; Carl Zeiss MicroImaging, Inc.) controlled by MetaView software (Universal Imaging Corp.) using a 40× or 100×/1.3 Plan-Neofluar oil objectives. When necessary, images were scanned using a piezo device adapted to a 100×/1.3 Plan-Neofluar objective and treated by deconvolution microscopy using a calculated point spread function.

Cell transfection
GFP–CLIP-170 cDNA was provided by F. Perez (Institut Curie, Paris, France); EB3-RFP was provided by V. Small (Institute of Molecular Biotechnology, Vienna, Austria); and GFP–CLIP-115 (Hoogenraad et al., 2000), EGFP–p150 Glued (Hoogenraad et al., 2001), GFP-CLASP1 (Akhmanova et al., 2001), and GFP-MCAK (Wordeman et al., 1999) have been described. Mouse TTL coding sequence was inserted in pcDNA3 (Invitrogen). CLIP-170–HD–YFP (aa 1–278) was generated in pCLink vector.

MEF cultures were transfected using 1 μg of DNA and Lipofectamine Plus (Invitrogen). For cotransfection experiments using RFP and GFP constructs, we used 1 μg of total DNA, and pilot transfections were performed to determine the respective proportion of each DNA, which led to transfected cells positive for both RFP and GFP. For rescue experiments, we performed cotransfection with GFP–CLIP-170 and TTL cDNA (ratio 1:4); the efficiency of the cotransfection was evaluated by the presence of both GFP–CLIP-170 protein and of Tyr tubulin (as a result of the presence of TTL). siRNA specific for α-tubulin were used as previously described (Erck et al., 2005).

Micropattern fabrication
L-shaped fibronectin micropatterns that were 35 μm long were made as described previously (Thery et al., 2005). MEFs were resuspended in DME 10% FBS and deposited on the printed coverslip at a density of 10^4 cells per cm^2.

Time-lapse video microscopy
To analyze MT growth rates, we cultured MEFs in 35-mm glass Petri dishes (Iwaki). 48 h after cotransfection with GFP–CLIP-170 and EB3-RFP cDNAs, cells were maintained in DME 10% FBS and placed in a humidified incubator at 37°C with 5% CO_2 inside the video microscopy platform. Fluorescent images were captured every 3 s with a charge-coupled device camera (CoolSNAP HQ; Roper Scientific) using a 100×/1.3 Plan-Neofluar oil objective in an inverted motorized microscope (Axiovert 200M; Carl Zeiss MicroImaging, Inc.) controlled by MetaMorph software (Universal Imaging Corp.). To measure MT growth rate, we quantified EB3-RFP velocity in >30 cells for each phenotype. To analyze mitotic spindle position, MEFs were plated on L-shaped fibronectin micropatterns and placed inside the video microscopy platform. Time-lapse images were collected every 3 min in multi-position in transillumination. To quantify mitotic angles, we designed a line perpendicular to the metaphase plate and measured the angle between this line and the micropattern hypotenuse using MetaMorph software.

Preparation of Tyr and Glu tubulin
Affinity-purified Tyr or Glu tubulin were prepared as previously described (Paturle et al., 1989). For storage (−80°C), both forms of tubulin were transferred to PEM buffer (pH 6.65, 100 mM Pipes, 1 mM EGTA, and 1 mM $MgCl_2$) made with D_2O instead of H_2O, containing 1 mM GTP and 10 mM $MgCl_2$.

Protein purification, MT polymerization, and cosedimentation assay
His–CLIP-170 HD (H1 fragment; aa 1–350; Scheel et al., 1999) cloned into pET19b vector was provided by F. Perez. His–p150 Glued HD (aa 46–253) and His-tagged EB1 (aa 1–268), both cloned into pET28 vector, were as described (Stepanova et al., 2003; Lansbergen et al., 2004). All constructs were expressed in bacteria, and proteins were purified as previously described. Tubulin was centrifuged for 10 min at 200,000 g, and polymerization was performed by incubating Tyr or Glu tubulin with His–CLIP-170 HD, with His–p150 Glued HD or with His-EB1 in PEM with 1 mM GTP, 5 mM $MgCl_2$, and 20% glycerol at 37°C for 20 min. 20 μM taxol was added for 10 min, and the presence of MTs was routinely checked using immunofluorescence microscopy or EM. Taxol-stabilized MTs were then exposed to increasing concentrations of NaCl (0, 100, 150, 200, and 300 mM in PEM 20% glycerol) for 10 min at 37°C. The reaction mixture was ultracentrifuged in a PEM 60% glycerol cushion for 30 min at 250,000 g at 30°C, and supernatants and pellets were analyzed by SDS-PAGE gels. More than five independent experiments were achieved with His–CLIP-170 HD and His–p150 Glued HD, Coomassie blue–stained gels were scanned with a scanner (PowerLook 1120; Umax), and bands were quantified using Image Quant software.

Online supplemental material
Fig. S1 shows GFP–CLIP-170 localization in WT or TTL-null fibroblasts. Video 1 shows MT growth rate in a WT fibroblast. Video 2 shows MT growth rate in a TTL-null CLIP+ fibroblast. Video 3 shows MT growth rate in a TTL-null CLIP– fibroblast. Online supplemental material is available at http://www.jcb.org/cgi/content/full/jcb.200512058/DC1.

References

Akhmanova, A., and C.C. Hoogenraad. 2005. Microtubule plus-end-tracking proteins: mechanisms and functions. *Curr. Opin. Cell Biol.* 17:47–54.

Akhmanova, A., C.C. Hoogenraad, K. Drabek, T. Stepanova, B. Dortland, T. Verkerk, W. Vermeulen, B.M. Burgering, C.I. De Zeeuw, F. Grosveld, and N. Galjart. 2001. Clasps are CLIP-115 and -170 associating proteins involved in the regional regulation of microtubule dynamics in motile fibroblasts. *Cell.* 104:923–935.

Badin-Larcon, A.C., C. Boscheron, J.M. Soleilhac, M. Piel, C. Mann, E. Denarier, A. Fourest-Lieuvin, L. Lafanechere, M. Bornens, and D. Job. 2004. Suppression of nuclear oscillations in *Saccharomyces cerevisiae* expressing Glu tubulin. *Proc. Natl. Acad. Sci. USA.* 101:5577–5582.

Barra, H.S., C.A. Arce, and C.E. Argarana. 1988. Posttranslational tyrosination/detyrosination of tubulin. *Mol. Neurobiol.* 2:133–153.

Brunner, D., and P. Nurse. 2000. CLIP170-like tip1p spatially organizes microtubular dynamics in fission yeast. *Cell.* 102:695–704.

Bulinski, J.C., D. Gruber, K. Faire, P. Prasad, and W. Chang. 1999. GFP chimeras of E-MAP-115 (ensconsin) domains mimic behavior of the endogenous protein in vitro and in vivo. *Cell Struct. Funct.* 24:313–320.

Busch, K.E., and D. Brunner. 2004. The microtubule plus end-tracking proteins mal3p and tip1p cooperate for cell-end targeting of interphase microtubules. *Curr. Biol.* 14:548–559.

Busson, S., D. Dujardin, A. Moreau, J. Dompierre, and J.R. De Mey. 1998. Dynein and dynactin are localized to astral microtubules and at cortical sites in mitotic epithelial cells. *Curr. Biol.* 8:541–544.

Carvalho, P., J.S. Tirnauer, and D. Pellman. 2003. Surfing on microtubule ends. *Trends Cell Biol.* 13:229–237.

Coquelle, F.M., M. Caspi, F.P. Cordelieres, J.P. Dompierre, D.L. Dujardin, C. Koifman, P. Martin, C.C. Hoogenraad, A. Akhmanova, N. Galjart, et al.

2002. LIS1, CLIP-170's key to the dynein/dynactin pathway. *Mol. Cell. Biol.* 22:3089–3102.

Culver-Hanlon, T.L., S.A. Lex, A.D. Stephens, N.J. Quintyne, and S.J. King. 2006. A microtubule-binding domain in dynactin increases dynein processivity by skating along microtubules. *Nat. Cell Biol.* 8:264–270.

Erck, C., L. Peris, A. Andrieux, C. Meissirel, A.D. Gruber, M. Vernet, A. Schweitzer, Y. Saoudi, H. Pointu, C. Bosc, et al. 2005. A vital role of tubulin-tyrosine-ligase for neuronal organization. *Proc. Natl. Acad. Sci. USA.* 102:7853–7858.

Faulkner, N.E., D.L. Dujardin, C.Y. Tai, K.T. Vaughan, C.B. O'Connell, Y. Wang, and R.B. Vallee. 2000. A role for the lissencephaly gene LIS1 in mitosis and cytoplasmic dynein function. *Nat. Cell Biol.* 2:784–791.

Fukata, M., T. Watanabe, J. Noritake, M. Nakagawa, M. Yamaga, S. Kuroda, Y. Matsuura, A. Iwamatsu, F. Perez, and K. Kaibuchi. 2002. Rac1 and Cdc42 capture microtubules through IQGAP1 and CLIP-170. *Cell.* 109:873–885.

Galjart, N., and F. Perez. 2003. A plus-end raft to control microtubule dynamics and function. *Curr. Opin. Cell Biol.* 15:48–53.

Gundersen, G.G. 2002. Microtubule capture: IQGAP and CLIP-170 expand the repertoire. *Curr. Biol.* 12:R645–R647.

Gundersen, G.G., and J.C. Bulinski. 1986. Microtubule arrays in differentiated cells contain elevated levels of a post-translationally modified form of tubulin. *Eur. J. Cell Biol.* 42:288–294.

Gundersen, G.G., M.H. Kalnoski, and J.C. Bulinski. 1984. Distinct populations of microtubules: tyrosinated and nontyrosinated alpha tubulin are distributed differently in vivo. *Cell.* 38:779–789.

Hayashi, I., A. Wilde, T.K. Mal, and M. Ikura. 2005. Structural basis for the activation of microtubule assembly by the EB1 and p150Glued complex. *Mol. Cell.* 19:449–460.

Haydar, T.F., E. Ang Jr., and P. Rakic. 2003. Mitotic spindle rotation and mode of cell division in the developing telencephalon. *Proc. Natl. Acad. Sci. USA.* 100:2890–2895.

Hoogenraad, C.C., A. Akhmanova, F. Grosveld, C.I. De Zeeuw, and N. Galjart. 2000. Functional analysis of CLIP-115 and its binding to microtubules. *J. Cell Sci.* 113:2285–2297.

Hoogenraad, C.C., A. Akhmanova, S.A. Howell, B.R. Dortland, C.I. De Zeeuw, R. Willemsen, P. Visser, F. Grosveld, and N. Galjart. 2001. Mammalian Golgi-associated Bicaudal-D2 functions in the dynein-dynactin pathway by interacting with these complexes. *EMBO J.* 20:4041–4054.

Huisman, S.M., and M. Segal. 2005. Cortical capture of microtubules and spindle polarity in budding yeast - where's the catch? *J. Cell Sci.* 118:463–471.

Komarova, Y.A., A.S. Akhmanova, S. Kojima, N. Galjart, and G.G. Borisy. 2002. Cytoplasmic linker proteins promote microtubule rescue in vivo. *J. Cell Biol.* 159:589–599.

Komarova, Y., G. Lansbergen, N. Galjart, F. Grosveld, G.G. Borisy, and A. Akhmanova. 2005. EB1 and EB3 control CLIP dissociation from the ends of growing microtubules. *Mol. Biol. Cell.* 16:5334–5345.

Kreis, T.E. 1987. Microtubules containing detyrosinated tubulin are less dynamic. *EMBO J.* 6:2597–2606.

Lafanechere, L., C. Courtay-Cahen, T. Kawakami, M. Jacrot, M. Rudiger, J. Wehland, D. Job, and R.L. Margolis. 1998. Suppression of tubulin tyrosine ligase during tumor growth. *J. Cell Sci.* 111:171–181.

Lansbergen, G., Y. Komarova, M. Modesti, C. Wyman, C.C. Hoogenraad, H.V. Goodson, R.P. Lemaitre, D.N. Drechsel, E. van Munster, T.W. Gadella Jr., et al. 2004. Conformational changes in CLIP-170 regulate its binding to microtubules and dynactin localization. *J. Cell Biol.* 166:1003–1014.

Maiato, H., A. Khodjakov, and C.L. Rieder. 2005. *Drosophila* CLASP is required for the incorporation of microtubule subunits into fluxing kinetochore fibres. *Nat. Cell Biol.* 7:42–47.

Mialhe, A., L. Lafanechere, I. Treilleux, N. Peloux, C. Dumontet, A. Bremond, M.H. Panh, R. Payan, J. Wehland, R.L. Margolis, and D. Job. 2001. Tubulin detyrosination is a frequent occurrence in breast cancers of poor prognosis. *Cancer Res.* 61:5024–5027.

Mimori-Kiyosue, Y., I. Grigoriev, G. Lansbergen, H. Sasaki, C. Matsui, F. Severin, N. Galjart, F. Grosveld, I. Vorobjev, S. Tsukita, and A. Akhmanova. 2005. CLASP1 and CLASP2 bind to EB1 and regulate microtubule plus-end dynamics at the cell cortex. *J. Cell Biol.* 168:141–153.

Mitchison, T.J. 1989. Polewards microtubule flux in the mitotic spindle: evidence from photoactivation of fluorescence. *J. Cell Biol.* 109:637–652.

Moore, A.T., K.E. Rankin, G. von Dassow, L. Peris, M. Wagenbach, Y. Ovechkina, A. Andrieux, D. Job, and L. Wordeman. 2005. MCAK associates with the tips of polymerizing microtubules. *J. Cell Biol.* 169:391–397.

Paturle, L., J. Wehland, R.L. Margolis, and D. Job. 1989. Complete separation of tyrosinated, detyrosinated, and nontyrosinatable brain tubulin subpopulations using affinity chromatography. *Biochemistry.* 28:2698–2704.

Paturle-Lafanechere, L., M. Manier, N. Trigault, F. Pirollet, H. Mazarguil, and D. Job. 1994. Accumulation of delta 2-tubulin, a major tubulin variant that cannot be tyrosinated, in neuronal tissues and in stable microtubule assemblies. *J. Cell Sci.* 107:1529–1543.

Perez, F., G.S. Diamantopoulos, R. Stalder, and T.E. Kreis. 1999. CLIP-170 highlights growing microtubule ends in vivo. *Cell.* 96:517–527.

Pollard, T.D., and G.G. Borisy. 2003. Cellular motility driven by assembly and disassembly of actin filaments. *Cell.* 112:453–465.

Scheel, J., P. Pierre, J.E. Rickard, G.S. Diamantopoulos, C. Valetti, F.G. van der Goot, M. Haner, U. Aebi, and T.E. Kreis. 1999. Purification and analysis of authentic CLIP-170 and recombinant fragments. *J. Biol. Chem.* 274:25883–25891.

Stepanova, T., J. Slemmer, C.C. Hoogenraad, G. Lansbergen, B. Dortland, C.I. De Zeeuw, F. Grosveld, G. van Cappellen, A. Akhmanova, and N. Galjart. 2003. Visualization of microtubule growth in cultured neurons via the use of EB3-GFP (end-binding protein 3-green fluorescent protein). *J. Neurosci.* 23:2655–2664.

Tanenbaum, M.E., N. Galjart, M.A. van Vugt, and R.H. Medema. 2006. CLIP-170 facilitates the formation of kinetochore-microtubule attachments. *EMBO J.* 25:45–57.

Thery, M., V. Racine, A. Pepin, M. Piel, Y. Chen, J.B. Sibarita, and M. Bornens. 2005. The extracellular matrix guides the orientation of the cell division axis. *Nat. Cell Biol.* 7:947–953.

Vasiliev, J.M., T. Omelchenko, I.M. Gelfand, H.H. Feder, and E.M. Bonder. 2004. Rho overexpression leads to mitosis-associated detachment of cells from epithelial sheets: a link to the mechanism of cancer dissemination. *Proc. Natl. Acad. Sci. USA.* 101:12526–12530.

Vaughan, K.T., S.H. Tynan, N.E. Faulkner, C.J. Echeverri, and R.B. Vallee. 1999. Colocalization of cytoplasmic dynein with dynactin and CLIP-170 at microtubule distal ends. *J. Cell Sci.* 112:1437–1447.

Wehland, J., and K. Weber. 1987. Turnover of the carboxy-terminal tyrosine of alpha-tubulin and means of reaching elevated levels of detyrosination in living cells. *J. Cell Sci.* 88:185–203.

Wordeman, L., M. Wagenbach, and T. Maney. 1999. Mutations in the ATP-binding domain affect the subcellular distribution of mitotic centromere-associated kinesin (MCAK). *Cell Biol. Int.* 23:275–286.

Yu, F., X. Morin, Y. Cai, X. Yang, and W. Chia. 2000. Analysis of partner of inscuteable, a novel player of *Drosophila* asymmetric divisions, reveals two distinct steps in inscuteable apical localization. *Cell.* 100:399–409.